Ref.TH.2436-CERN

BARYON-ANTIBARYON BOUND STATES AND ANNIHILATION

B.R. Karlsson and B. Kerbikov *)
CERN - Geneva

A B S T R A C T

In order to gain some insight into the problem of the widths of quasi-nuclear levels in the $B\bar{B}$ systems, we investigate a simple multichannel model for the influence of decay channels on a bound state. The shift and width of a bound state level is found to depend strongly not only on the range of the annihilation and the $B\bar{B}$ wave function at small distances but also on the position of the level relative to the thresholds. We point out a new mechanism through which a level in the vicinity of open thresholds can remain narrow even for strong coupling to the decay channels.

---

*) On leave of absence from the Institute of Theoretical and Experimental Physics, Moscow.

Ref.TH.2436-CERN
9 December 1977

1. INTRODUCTION

It is now well known that the nuclear forces in the nucleon-antinucleon system are strong enough to generate a family of quasi-nuclear bound states[1-4]. Such states are unstable against annihilation and they might therefore only manifest themselves as broad structures, if at all. However, more detailed investigations[1,5] have led to the prediction that the quasi-nuclear levels will in fact remain rather narrow, with widths in the range 0.1-100 MeV (depending on their orbital angular momentum, the short-range behaviour of the $\bar{N}N$ force, etc.). This stability of the spectrum comes from the short-range character of the annihilation process: if, following Martin[6], this range is taken equal to half the Compton wavelength of the nucleon, $\simeq 0.1$ fm, and the radius of the $N\bar{N}$ state is ≈ 1 fm, only a small fraction of the $N\bar{N}$ wave function is in the annihilation region.

On the contrary, and on the basis of a calculation using a simple imaginary potential to represent annihilation, it has been claimed[7,8] that only very few $N\bar{N}$ states have a chance to remain narrow (see, however, also Ref. 5).

Experimentally, there has been considerable progress during the last few years, and there are now about 10 candidates for narrow quasi-nuclear states[9].

In general, a multichannel model would be expected to be able to represent the annihilation in the $N\bar{N}$ system (or any other $B\bar{B}$ system) in a better way than an *ad hoc* optical potential. In this note we will show that already a very simple multichannel model gives results which are very different from those obtained in Refs. 7 and 8. In particular, we find that a strong coupling to an annihilation channel does not necessarily lead to a drastic broadening of the quasi-nuclear $B\bar{B}$ state. The model we will use is a generalized and more detailed version of the two-channel model recently discussed for the same physical problem in Ref. 10.

In the following we will apply this model to the $B\bar{B}$ system, but the results are in most cases general and should apply to any physical system with a bound state affected by decay.

2. A COUPLED CHANNEL MODEL FOR ANNIHILATION

In order to expose the essential features of the model, we will make several simplifying assumptions, namely:

i) particles in all channels are non-relativistic, spinless, and in relative s-states;

ii) all decay channels are of quasi-two-body type, and coupled only to the $B\bar{B}$ channel (i.e. not to each other);

iii) the particles in the decay channels are non-interacting.

The Hamiltonian corresponding to this model has the matrix form H + V, where (index 1 is used for the $B\bar{B}$ channel)

$$H_{11} = \frac{k_1^2}{m_1} + U \; ; \qquad H_{ii} = \frac{k_i^2}{m_i} - 2(m_1 - m_i) \; , \quad i = 2, 3, \ldots, N. \tag{1}$$

and $H_{ij} = 0$, $i \neq j$. Here U is the $B\bar{B}$ potential which creates the bound state to be investigated. To simplify the notation we have taken the masses m_i of the two particles in channel i to be equal, with all $m_i < m_1$; m_1 is the B particle mass. The matrix V describes the coupling to the annihilation channels. According to (iii), its only non-vanishing matrix elements are V_{1j} and $V_{j1} = V_{1j}^{+}$, $j = 2, 3, \ldots, N$, and we choose these in a simple separable form:

$$V_{1j} = \lambda_j \, |\beta_1\rangle\langle\beta_j| \tag{2}$$

where the λ_j's should be real. The form factors are taken as

$$\langle r_j|\beta_j\rangle = \sqrt{2\beta_j}\, r_j^{-1} \exp(-\beta_j r_j) \; , \qquad \langle \beta_j|\beta_j\rangle = 1 \; , \; j = 1, 2, \ldots, N. \tag{3}$$

The Schrödinger equation corresponding to this Hamiltonian can easily be solved (algebraically), and we find the following eigenvalue equation for the energy E

$$1 - \langle\beta_1|G_1(E)|\beta_1\rangle \sum_{j>1}^{N} \lambda_j^2 \langle\beta_j|G_j(E)|\beta_j\rangle = 0 \tag{4}$$

in terms of the channel Green's functions $G_i(E) = (H_{ii} - E - i\varepsilon)^{-1}$. [Equation (4) is more precisely the condition for the vanishing of the denominator function in an N/D representation for the multichannel T-matrix[11)]] .

Recalling assumption (iii), the matrix elements in (4) corresponding to $j \neq 1$ can be calculated explicitly:

$$\langle\beta_j|G_j(E)|\beta_j\rangle = m_j (\beta_j - i k_j)^{-2} . \tag{5}$$

The momentum $k_j = \{m_j [2(m_1 - m_j) + E]\}^{\frac{1}{2}}$ in channel j is related to $k_1 = (m_1 E)^{\frac{1}{2}}$ through the kinematical condition

$$k_j^2 = \rho_j \left[2 m_1^2 (1 - \rho_j) + k_1^2 \right], \tag{6}$$

where $\rho_j = m_j/m_1 < 1$.

The general structure of the matrix element $\langle \beta_1 | G_1(E) | \beta_1 \rangle$ in Eq. (4) as a function of E, or k_1, is that of the inverse of the Jost function in channel 1, $\mathcal{L}^{-1}(k_1)$, with some additional singularities coming from the form factors $|\beta_1\rangle$. This can be seen using the representation[12)]

$$G_1(k; r, r') = m_1 (r_1 r_1')^{-1} f_+(k, r_>) \varphi(k, r_<) \mathcal{L}^{-1}(k)$$

for $G_1(E)$, where $\phi(k,r)$, and $f_+(k,r)$ are the regular and the Jost solutions to the Schrödinger equation, respectively. In particular, a bound state in channel 1 with energy $-|E_0| = -\kappa_0^2/m_1$ is associated with a pole at $k_1 = i\kappa_0$. The residue of $\langle \beta_1 | G_1(E) | \beta_1 \rangle$ at this pole is equal to $i(m_1/2\kappa_0) |\langle \beta_1 | \phi \rangle|^2$, as is easily seen using the bound-state part $|\phi\rangle (-|E_0| - E)^{-1} \langle \phi|$ of the spectral representation of G_1 *). Using the Hultén form for the bound state wave function

$$\langle r | \varphi \rangle = \sqrt{\frac{2\alpha\kappa_0(\alpha+\kappa_0)}{(\kappa_0-\alpha)^2}} \left[\exp(-\kappa_0 r) - \exp(-\alpha r) \right] / r, \tag{7}$$

we can also get an explicit expression for $|\langle \beta_1 | \phi \rangle|^2$.

It is not sufficient for our purposes to approximate $\langle \beta_1 | G_1(E) | \beta_1 \rangle$ by this pole term alone, but a contribution from the continuous spectrum must also be included. A consistent way of doing this is to replace the true potential U by a separable potential $-\eta |\alpha\rangle\langle\alpha|$ with the form factor $|\alpha\rangle = (H_{11} - U + |E_0|) |\phi\rangle$. Such a potential reproduces not only the bound state energy but also the bound state wave function. For the Hulthén wave function, the form factor $\langle r | \alpha \rangle$ has the form (3) with β_j substituted by α. The resulting expression for $\langle \beta_1 | G_1(E) | \beta_1 \rangle$ is given in the Appendix. In the neighbourhood of the pole it can be reduced to

$$\langle \beta_1 | G_1(E) | \beta_1 \rangle \simeq \frac{m_1 \beta_1}{(\beta_1 + \kappa_0)^2 (\beta_1 + \alpha)} \left[1 + i \frac{2\alpha(\kappa_0 + \alpha)}{(k_1 - i\kappa_0)(\beta_1 + \alpha)} \right]. \tag{8}$$

---

*) The spectral representation suggests that there is also a pole at $k_1 = -i\kappa_0$. This is however not the case, since $\mathcal{L}^{-1}(k_1)$ has no singularity at this point.

Equation (A.1) is expected to give a good representation of $\langle\beta_1|G_1(E)|\beta_1\rangle$ to the extent that other dynamical singularities (e.g. other bound states or resonance poles) are far away from the pole under investigation.

To conclude the general description of our model, let us make some comments on the parameters that have been introduced. In the $N\bar{N}$ case, m_1 is the nucleon mass. The assumption of non-relativistic motion requires the masses m_i to be chosen in such a way that $0.5 \ll m_i/m_1 < 1$, and $|E_0|$ to be less than a few hundred MeV, i.e. $\kappa_0 = \sqrt{m_1|E_0|} \lesssim 500$ MeV/c. The parameter α can be used to vary the size of the $B\bar{B}$ system (unless the binding is small), or the value of the wave function at the origin (i.e. in the annihilation region). If the β_j's, which determine the size of the annihilation region, are taken equal to $2m_1$, then α/β_j will be typically of the order of 1/10. The coupling constants λ_j will be treated as free parameters. For a given physical system they can be constrained, e.g. by the annihilation cross-section in the $B\bar{B}$ channel. In the two-channel version of our model (with $\lambda_2 = \lambda$ and $\beta_1 = \beta_2 = \beta$) the T-matrix for annihilation is given by

$$\langle 2 | T_{21} | 1 \rangle = \langle \psi_2^- | \beta \rangle \frac{\lambda}{\mathfrak{D}(E)} \langle \beta | \psi_1^+ \rangle$$

where $\mathfrak{D}(E) = 1-\lambda^2 \langle \beta|G_1(E)|\beta \rangle \langle \beta|G_2(E)|\beta\rangle$ and where $|\psi^{\pm}\rangle$ are eigenchannel scattering wave functions. The matrix element $|\langle 2|T_{21}|1\rangle|$ vanishes when $\lambda \to 0$ or $\lambda \to \infty$ and has its maximum value when $\lambda = |\langle\beta|G_1(E)|\beta\rangle\langle\beta|G_2(E)|\beta\rangle|^{-\frac{1}{2}}$. For $E \approx 0$ and with $\beta \sim 2m_1$, $\alpha/\beta \ll 1$ and $\alpha/\kappa_0 \lesssim 1$ we find approximatively $\lambda/\sqrt{m_1 m_2} \sim 4$. For λ-values beyond the maximum, a bound state initially in channel 1 is so strongly coupled to the other channel that the model (e.g. with no interaction in channel 2) is no longer realistic. Another natural bound on the magnitude of λ comes from the observation that large enough λ will create poles near the physical region that are due to the off-diagonal interaction alone (compare footnote in Section 4). When this happens, the coupling to the annihilation channel is again so strong that the system is no longer predominantly of the $B\bar{B}$ type.

To conclude this section, we recall some general properties of the multi-channel S-matrix[12] that are of some relevance for the description of decay channel effects on a bound-state pole. As a function of energy, S has a branch point at every threshold $E = -2(m_1-m_i)$, $i = 1, 2, \ldots, N$. All these branch points are present on each sheet so that the Riemann surface of S has 2^N sheets. The physical sheet is characterized by having all momenta $k_1, k_2, \ldots, k_N$ in their upper half planes. S has no poles in the physical sheet, except for bound-state poles on the real axis. A single narrow resonance is characterized by one pair of poles on each non-physical sheet, in all 2^N poles. If the parameters of the theory (coupling constants, etc.) are varied, a resonance peak will sometimes be associated with one, sometimes with another of these poles (see, for example, Ref. 13).

If S is considered as a function of the k_j's, the Riemann surface has 2^{N-1} sheets, as can be seen from our Eq. (6).

In the two-channel case, the cut between the two branch-points $\pm im_1\sqrt{2(1-\rho_2)}$ in the k_1-plane is normally taken along the imaginary axis as in Fig. 1. Correspondingly, in the k_2-plane there are two cuts along the real axis from the points $\pm m_1\sqrt{2\rho_2(1-\rho_2)}$ to $\pm\infty$ as in Fig. 4 (disregarding the cut along the imaginary axis which in this case is generated by a third channel). The Riemann surface of the two-channel S-matrix as a function of energy has four sheets, usually labelled according to Peierls[12]: Im $k_1 > 0$ on sheets I (physical) and II, and Im $k_2 > 0$ on sheets I and IV, see Fig. 1.

3. THE INFLUENCE OF DISTANT THRESHOLDS ON A BOUND STATE

Using the framework outlined in the preceding section we now proceed to investigate the motion of the bound-state pole away from $E = -|E_0|$ as the coupling to the annihilation channels is gradually switched on. Explicitly, we want to solve Eq. (4) for E as a function of the λ_j's. We first consider the case of only one decay channel with the corresponding threshold far from the initial position of the bound state (we take $\beta_1 = \beta_2 \equiv \beta$ and $\lambda_2 \equiv \lambda$). More precisely, we assume that

$$2(m_1 - m_2) \gg \beta_2^{-1}(2+\beta_2)\,\max\left(|E_0|, \alpha^2 m_1^{-1}\right). \tag{9}$$

Under this condition, far away singularities in Eq. (4) can be considered as fixed ($k \to i\kappa_0$). Combining Eqs. (4), (5), and (8) we therefore find for the pole position as a function of λ^2

$$\frac{1}{\lambda^2} = \frac{m_1 m_2 \beta}{(\beta+\kappa_0)^2(\beta-ik_{20})^2(\beta+\alpha)}\left[1 + i\frac{2\alpha(\kappa_0+\alpha)}{(k_1-i\kappa_0)(\beta+\alpha)}\right], \tag{10}$$

where $k_{20}^2 = \rho_2\left[2m_1^2(1-\rho_2) - \kappa_0^2\right]$. Equation (10) can be thought of as the conformal mapping of the half-line $\lambda^2 \in [0,\infty)$ onto a circular arch in the k_1-plane. The equation for the circle is obtained by putting $k_1 - i\kappa_0 = iR\,e^{i\phi}$ and taking the imaginary part of Eq. (10):

$$R = \frac{2\alpha(\kappa_0+\alpha)}{(\beta+\alpha)\sin\chi}\sin(\phi-\chi), \tag{11}$$

where $\sin\chi = 2\beta k_{20}(\beta^2 + k_{20}^2)^{-1}$. The interval $\lambda^2 \in [0,\infty)$, corresponds to $\phi \in [\chi,\pi)$, and this part of the circle lies in sheet II and possibly sheet IV (Fig. 1), with the end points on the imaginary k_1-axis. The corresponding trajectory in the energy plane follows from the equation

$$\Delta E = E - E_0 = -m_1^{-1} R \exp(i\phi)\left[2\varkappa_0 + R\exp(i\phi)\right], \quad (12)$$

where $\phi \in [\chi,\pi)$, and $\phi = 0$ is a ray antiparallel to the real axis (see Fig. 2). The maximum value of the energy displacement can easily be evaluated by combining Eqs. (11) and (12). If, for instance, β is large as compared to k_{20} and α, and $|E_0|$ is not too small, we find to a good approximation

$$|\Delta E|_{max} \simeq \left(\frac{m_1}{k_{20}}\right) \cdot \frac{2\alpha\varkappa_0(\varkappa_0+\alpha)}{m_1^2} \quad (13)$$

From formula (9),

$$m_1/k_{20} < \frac{1}{2}\sqrt{\frac{2+g_2}{g_2(1-g_2)}} < \frac{1}{\sqrt{2}}\, m_1/\alpha ,$$

where in the $N\bar{N}$ case the upper limit is typically ~ 5. In terms of the Hulthén wave function at the origin [see formula (7)], Eq. (13) can be written

$$|\Delta E|_{max} \simeq \frac{m_1}{k_{20}} \cdot \frac{|\langle 0|\varphi\rangle|^2}{m_1^2} \quad (14)$$

Our estimate for the maximum energy displacement is therefore similar to that obtained in Ref. 5 from different considerations.

As may be seen from Eq. (12) or Fig. 2, it can happen that Re E > 0 with Im E small. Such pole positions in sheets II and IV do not give rise to a resonance in the $B\bar{B}$ channel: for this to happen, we need a pole in sheet III close to the real axis.

The pole trajectory described in Fig. 2, left case, has previously been found in a numerical investigation of essentially the same model as that considered in this section[10]. In this connection it was also pointed out that Re ΔE is negative for small λ^2 provided $\beta^2 > k_{20}^2$. In our notation, small λ^2 corresponds to ϕ just above χ, and small R, so that [from Eq. (12)] Re $\Delta E \simeq -2R\varkappa_0 m_1^{-1} \cos\phi$. This expression is negative for $\phi \gtrsim \chi$ provided $\chi < \pi/2$ i.e. again if $\beta^2 > k_{20}^2$. Recalling the definition of k_{20} we can easily verify that

$$k_{20}^2 \leq \frac{m_1^2}{2}\left(1 - \frac{\varkappa_0^2}{2m_1^2}\right) < \frac{m_1^2}{2}$$

The condition $\chi < \pi/2$ is therefore always satisfied if $\beta^2 > m_1^2/2$, in particular if $\beta \gtrsim 2m_1$ as in the $N\bar{N}$ case.

We finally note that our two-channel model corresponds to an optical potential in channel 1, of the form

$$V_{opt} = -\lambda^2 |\beta\rangle\langle\beta| G_2(E) |\beta\rangle\langle\beta| = -\lambda^2 |\beta\rangle (\beta^2 + k_{20}^2)^{-1} \exp(i\chi) \langle\beta| \tag{15}$$

This potential is purely imaginary if $\chi = \pi/2$, i.e. if $\beta^2 = k_{20}^2$. In view of the above estimates on k_{20}, this can only happen if $\beta^2 < m_1^2/2$. Therefore, in the multi-channel model with the condition (9) we can never obtain a purely imaginary optical potential with an annihilation range $\sim \beta^{-1}$ smaller than $\sqrt{2}/m_1$ (~ 0.3 fm in the $N\bar{N}$ case). An imaginary potential similar to (15) was investigated numerically in Ref. 8, and the pole motion described in this reference corresponds in fact to a fairly circular trajectory in the momentum plane[14]. However, since p-wave form factors were used, and the α/β ratio was not small, the results of this reference cannot be directly compared to ours. In particular, it is not clear whether the parameters chosen are consistent with the assumption of an underlying (p-wave) multichannel model, e.g. of the type considered in this paper; or if so, that they correspond to reasonable values for, for example, the m_i's.

The picture outlined in this section remains the same also in the more general case of several annihilation channels provided the basic condition (9) applies to each one of them and the ratios between the coupling constants λ_j are kept constant. In such a case the only change is that the factor $(\beta - ik_{20})^{-2} = (\beta^2 + k_{20}^2)^{-1} \exp(i\chi)$ in formula (10) must be replaced by

$$\sum_{j>1} c_j (\beta_j^2 + k_{j0}^2)^{-1} \exp(i\chi_j) \equiv C' \exp(i\tilde{\chi})$$

with $c_j = \lambda_j^2/\lambda^2 = \text{const}$, and χ by $\tilde{\chi}$ in the subsequent formulae. In particular we note that $\tilde{\chi}$ is larger than the smallest of the χ_j's. Therefore, if all β_j's are the same, the *maximum* energy shift in the case of several channels is less than the shift produced by the most nearby channel alone.

4. THE INFLUENCE OF NEARBY THRESHOLDS ON A BOUND STATE

As the next case we consider a bound-state pole in the immediate vicinity of the last open threshold. We again use the two-channel model, but instead of condition (9) we now assume that the $B\bar{B}$ threshold is far away. The motion of the

pole is then most simply followed in terms of the momentum k_2 of the light particles. Introducing this variable into Eq. (4), and putting $k_1 = i\kappa_0$ in slowly varying factors, we obtain the equation

$$\frac{1}{\lambda^2} = \frac{m_1 m_2 \beta}{(\beta - ik_2)^2(\beta+\kappa_0)^2(\beta+\alpha)}\left[1 - g_2 \frac{4\alpha\kappa_0(\alpha+\kappa_0)}{(\beta+\alpha)(k_2^2 - k_{20}^2)}\right] \tag{16}$$

for k_2 as a function of λ^2. If we also neglect the small momentum k_2 as compared to β in the factor $(\beta - ik_2)$, the poles initially at $\pm k_{20}$ will with increasing λ^2 approach each other along the real axis, collide at the origin, and turn into a pair of poles moving away from each other along the imaginary axis, the upper one being in the physical sheet and corresponding to a bound state. If k_2 is kept in $(\beta - ik_2)$, the poles will instead approach each other along curves in sheet II, then collide on the imaginary axis and continue to move along this axis in opposite directions. The upper pole is of course again the physically more interesting*). This picture of pole motion is already familiar from one-channel potential theory: a pair of resonance poles move with increasing strength of the potential towards the imaginary k-axis, collide, and turn into two poles moving along this axis, one of them eventually becoming a bound-state pole. In Fig. 3 we indicate the energy plane trajectory of the more interesting pole motion found in this case.

Let us finally consider a three-channel model with the initial bound state just above the intermediate threshold (we put $\lambda_j^2 = \lambda^2 C_j$, $j = 2, 3$, and $\beta_1 = \beta_2 = \beta_3 \equiv \beta$). Expressing Eq. (4) in terms of the variable k_2 we find (with $k_1 = i\kappa_0$ in slowly varying factors)

$$\frac{1}{\lambda^2} = \frac{m_1 \beta}{(\beta+\kappa_0)^2(\beta+\alpha)}\left[1 - g_2 \frac{4\alpha\kappa_0(\kappa_0+\alpha)}{(\beta+\alpha)(k_2^2 - k_{20}^2)}\right] \times \left[C_2 \frac{m_2}{\beta^2} + C_3 \frac{m_3}{(\beta - ik_{30})^2}\right] \tag{17}$$

This equation has the same structure as Eq. (10): the pole trajectory as a function of λ^2 is circular, but this time in the k_2^2-plane, i.e. in the energy plane. In the k_2-plane there are therefore two poles, corresponding to $k_2 = \pm\sqrt{k_2^2}$, one in sheet III′ and the other in II′ (Fig. 4) (the labelling of sheets is similar

---

*) The pole going downwards will in this model collide with one of the poles coming from the $(\beta - ik_2)^2$ factor roughly at $k_2 \simeq -i\beta/2$. After the collision the resulting two poles eventually (when $\lambda^2 \to \infty$) return to the real k_2-axis along extended curves in the second sheet. These poles cannot mainly be associated with the forces in the $B\bar{B}$ channel but are rather induced by transitions between closed and open channels.

to that in Fig. 1, with $k_1 \to k_2$ and $k_2 \to k_3$). We note that for small λ^2 the pole in sheet III′ is closest to the physical region, while for large λ^2 the other pole takes over this role*).

Also the energy plane trajectory (Fig. 5) corresponds to the motion of two poles on different sheets. The one starting from the upper rim of the k_2 cut and going down through this cut into sheet III′ is for small λ^2 the physically more interesting. For larger λ^2, however, the pole starting on the lower rim of the k_2 cut and moving in sheet II′ becomes the physically relevant one, as before.

In a better approximation, the term $c_2 m_2/\beta^2$ in Eq. (17) should be kept in the form $c_2 m_2/(\beta \mp ik_2)^2$, where the upper (lower) sign corresponds to the solution in sheet III′ (II′). As a result, the II′-sheet trajectory is moved towards and the III′-sheet trajectory is moved away from the real axis in the energy plane.

5. RESULTS OF A NUMERICAL CALCULATION

In Fig. 6 we show the results of a few numerical solutions of the three-channel model using Eq. (4) together with Eqs. (5) and (A.1). All curves correspond to the same set of parameters m_1 = 940 MeV, m_2 = 820 MeV, m_3 = 770 MeV, α = 200 MeV/c $\sim 1\,\mathrm{fm}^{-1}$ and β = 1880 MeV/c $\sim 10\,\mathrm{fm}^{-1}$, and only the initial position of the bound state has been varied. The $|E_0|$ = 1 MeV curve corresponds to an almost perfect circle in the k_1-plane, while the 30 MeV curve is slightly distorted.

The 200 MeV trajectory has been chosen to illustrate a particularly interesting effect. In the second threshold region there are (in accord with the general discussion in Section 4) two trajectories of interest, both essentially circular. Since the third threshold is not very far away, the effective angle between these trajectories and the real axis is small, and the radii of the circles are large; in fact, the trajectories almost look like straight lines. As a consequence, the (upper trajectory) pole escapes the second threshold region well before it has a chance to get very far from the real axis. But once in the third threshold region, its behaviour is as foreseen (Fig. 3) for a pole in the neighbourhood of the last open threshold. Therefore, we have in this case an energy level with a small width for all values of the coupling to the annihilation channels.

---

*) This phenomenon is familiar in particular from a discussion of resonance pole motion as a function of SU(3) symmetry-breaking in the 1960's; see, for example, Ref. 13.

Intuitively, the pole behaviour seen in this example reflects the fact that when a level goes below a threshold, the corresponding decay channel does not increase the width any further. The description given above will therefore also be valid in the multichannel case, with the second theshold picture repeated at each open threshold. If in particular the initial pole position is not too far from the region of dominating decay channel thresholds, the sequence of pole trajectories will also in this case remain close to the real axis in the energy plane.

6. SUMMARY AND CONCLUSIONS

The simple multichannel model presented above has displayed some features of $B\bar{B}$ bound-state annihilation that have not been given much attention before. We have in particular seen that the widths of the levels are not only determined by the range of annihilation and the $B\bar{B}$ wave function at small distances, but that also the positions of the decay thresholds play an important role. For a single bound state well above all decay thresholds the displacement of the S-matrix pole due to annihilation (and therefore also the width of the level) has been explicitly found in terms of the parameters of the model. The trajectory of the pole as a function of the coupling to the annihilation channels is circular in the complex momentum plane and in qualitative agreement with the results of earlier numerical calculations[10]. There is a maximum value for the width of the level (as a function of the coupling), which is simply related to the bound-state wave function at the origin and to the distance to the next annihilation threshold.

The picture is different for a bound state in the vicinity of an annihilation threshold. When the coupling to the decay channels is gradually increased, the state is mainly shifted towards lower energy (larger binding) with only a small increase in the width. Several successive thresholds can therefore give such a state a chance to remain narrow even when the coupling to the annihilation channels gets strong. We think that this is a promising mechanism for narrow quasinuclear $N\bar{N}$ states, which should be further investigated using more specific information on the $N\bar{N}$ forces, the threshold positions, etc.

It might finally be recalled that the above results have been obtained for $\ell = 0$ bound states, i.e. without the help of angular momentum barriers to reduce the magnitude of the annihilation effects.

Acknowledgements

One of us (B. K.) is most grateful for the hospitality of the CERN Theory Division.

REFERENCES

1) I.S. Shapiro, Soviet Phys. Uspekhi 16, 173 (1973).
L.N. Bogdanova et al., Ann. Phys. (USA) 84, 261 (1974).

2) C.B. Dover and M. Goldhaber, Phys. Rev. D 15, 1997 (1977).

3) J.M. Richard et al., Phys. Letters 64B, 121 (1976).
R. Vinh Mau, IPNO/TH 77-14 (1977).

4) F. Myhrer, Preprint CERN TH 2348 (1977), talk at the 2nd Internat. Conf. on Nucleon-Nucleon Interactions, Vancouver, June 1977.

5) I.S. Shapiro, Preprint ITEP-88 (1977).

6) A. Martin, Phys. Rev. 124, 614 (1961).

7) F. Myhrer and A. Gersten, Nuovo Cimento 37A, 21 (1977).

8) F. Myhrer and A.W. Thomas, Phys. Letters 64B, 59 (1976).

9) L. Montanet, CERN/EP/Phys. 77-22, Paper submitted to the 5th Internat. Conf. on Experimental Spectroscopy, Boston, 29-30 April 1977.
S. Nilsson, Narrow resonances in BB reactions, 15th Course: The ways of sub-nuclear Physics, "Ettore Majorana" Centre for Scientific Culture, Erice, Sicily, 23 July-10 August 1977.
P. Pavlopoulos et al., Phys. Letters 72B, 415 (1978).

10) B. Kerbikov et al., Zh. Eksper. Theor. Fiz. Pis'ma 26, 505 (1977).

11) J.D. Bjorken, Phys. Rev. Letters 4, 473 (1960).

12) R.G. Newton, Scattering theory of waves and particles (McGraw-Hill, Inc., N.Y., 1966).
R.E. Peierls, Proc. Roy. Soc. A 253, 16 (1959).
R.J. Eden and J.R. Taylor, Phys. Rev. B 133, 1575 (1964).
M. Kato, Ann. Phys. (USA) 31, 130 (1965).

13) M. Ross, Phys. Rev. Letters 11, 450 and 567 (1963).
D. Amati, Phys. Letters 7, 290 (1963).
T. Kawai and N. Masuda, Nuovo Cimento 32, 243 (1964).
R.H. Dalitz and Rajasekaran, Phys. Letters 7, 373 (1963).

14) F. Myhrer, private communication.

APPENDIX

We want to calculate $\langle\beta|G_1(E)|\beta\rangle$, where $G_1 = (H_{11} + U - E - i0)^{-1}$, $U = -\eta|\alpha\rangle\langle\alpha|$, and where η has been chosen so as to give a bound state at $E = -|E_0| = -\kappa_0^2/m_1$. From the relation $G_1 = G_1^0 - G_1^0 U G_1$, with $G_1^0 = (H_{11} - E - i0)^{-1}$ we easily find $G_1 = G_1 - G_1^0|\alpha\rangle d^{-1}\langle\alpha|G_1^0$, where $d = \langle\alpha|G_1^0(E)|\alpha\rangle - 1/\eta =$ $= \langle\alpha|G_1^0(E)|\alpha\rangle - \langle\alpha|G_1^0(-|E_0|)|\alpha\rangle$. Using Eq. (5) and a similar result for $\langle\beta|G_1^0|\alpha\rangle$, we obtain

$$\langle\beta|G_1(E)|\beta\rangle = \frac{m_1}{(\beta - ik_1)^2}\left[1 - i\frac{2\alpha(\kappa_0+\alpha)}{(\beta+\alpha)(k_1+i\kappa_0+2i\alpha)}\right]\times\left[1 + i\frac{2\alpha(\kappa_0+\alpha)}{(\beta+\alpha)(k_1-i\kappa_0)}\right]$$

In the neighbourhood of the bound-state pole the first two factors in (A.1) are slowly varying functions of k; taking $k = i\kappa_0$ in these factors we get the simpler expression (8).

Figure captions

Fig. 1 : Momentum plane trajectory of the $B\bar{B}$ pole as a function of λ. The initial position far from annihilation thresholds.

Fig. 2 : Same as Fig. 1, but in energy plane.

Fig. 3 : $B\bar{B}$ pole trajectory as a function of λ. The initial position close to the last open threshold.

Fig. 4 : Momentum plane trajectory of the $B\bar{B}$ pole as a function of λ. The initial position close to an annihilation threshold (not the last open one).

Fig. 5 : Same as Fig. 4, but in energy plane.

Fig. 6a : $B\bar{B}$ pole trajectories as a function of λ, as obtained from the numerical solution of a three-channel model. The different trajectories correspond to different choices of initial pole position, the arrow corresponds to $\lambda/m_1 = 3$.

Fig. 6b : See Fig. 6a.

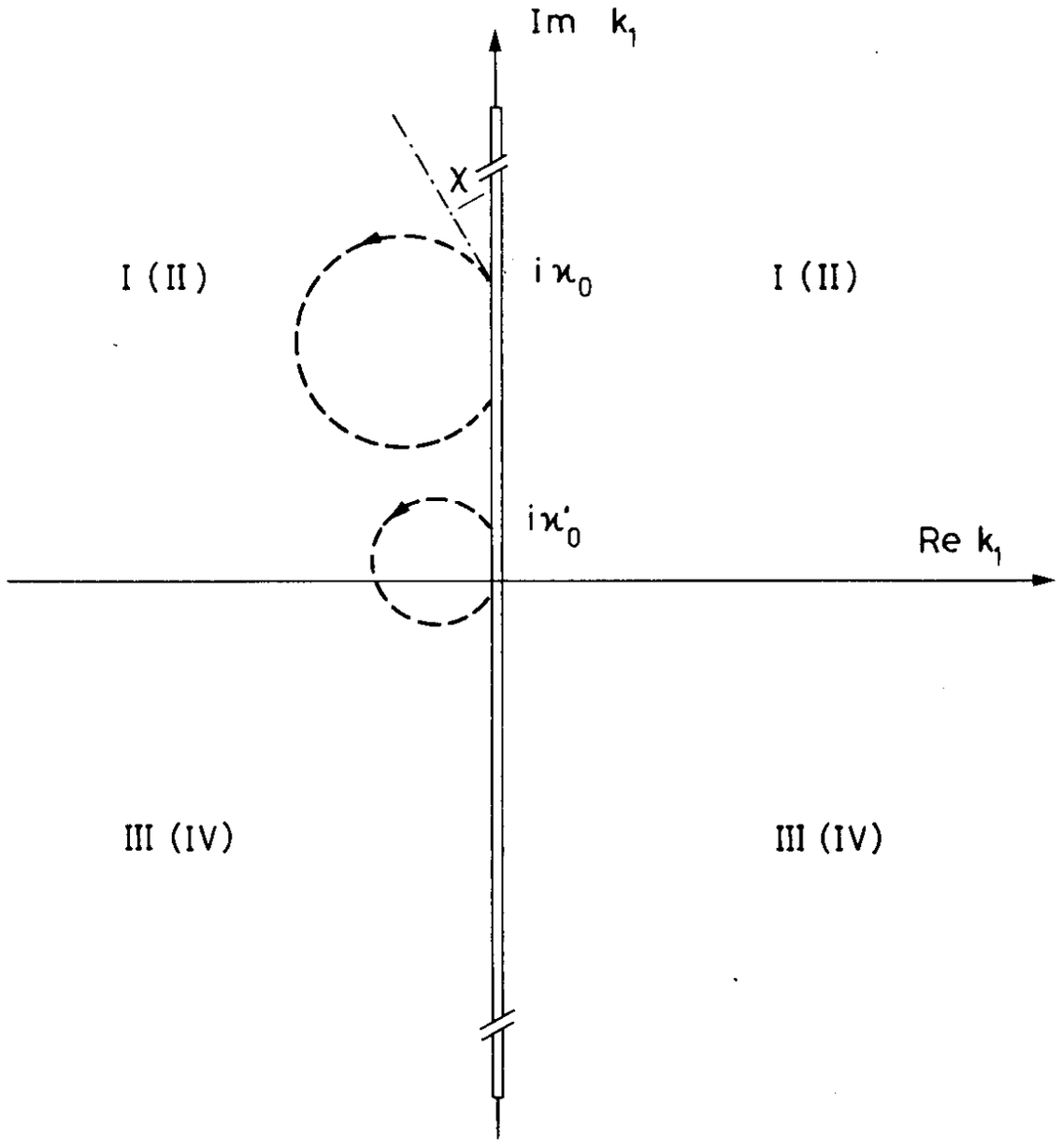

Fig. 1.

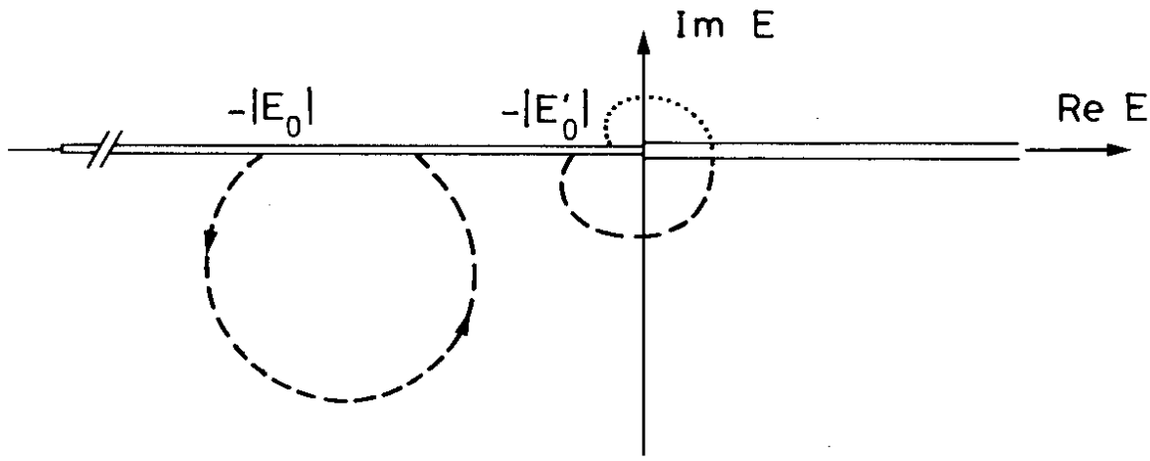

Fig. 2

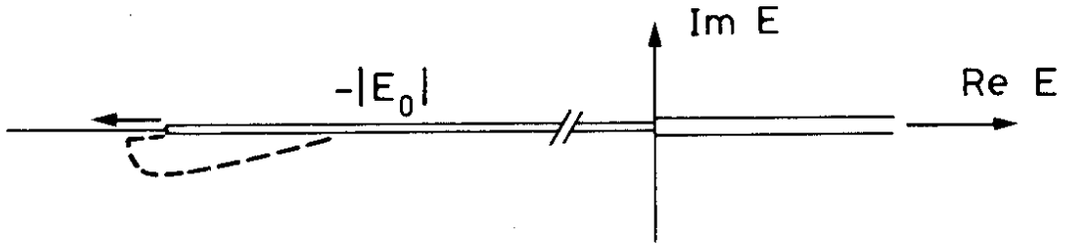

Fig. 3

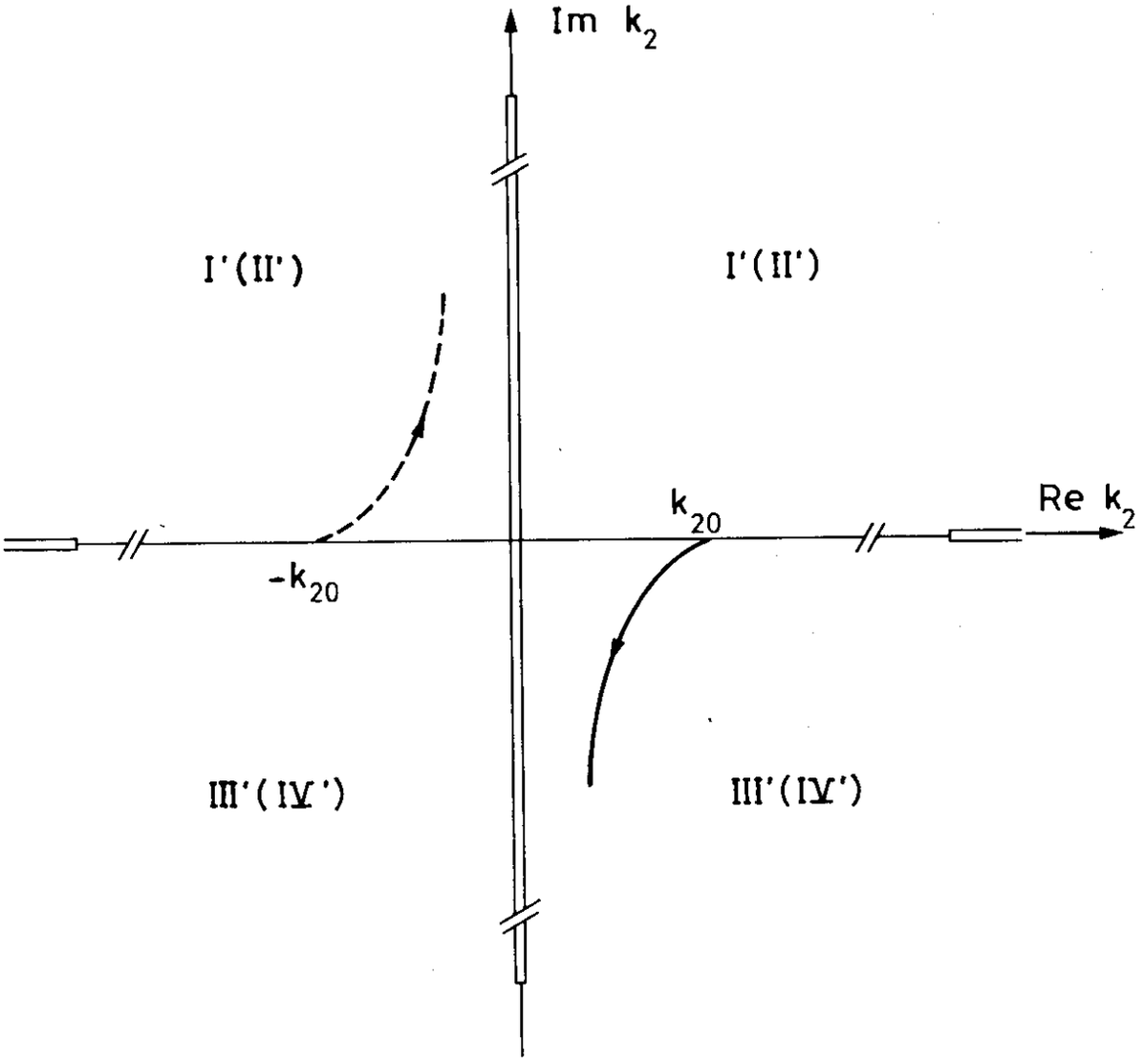

Fig. 4

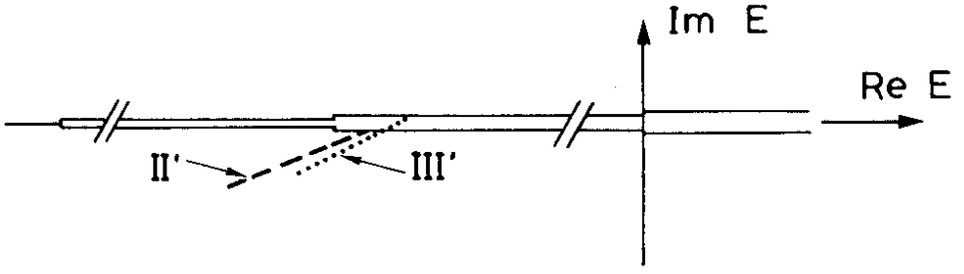

Fig. 5

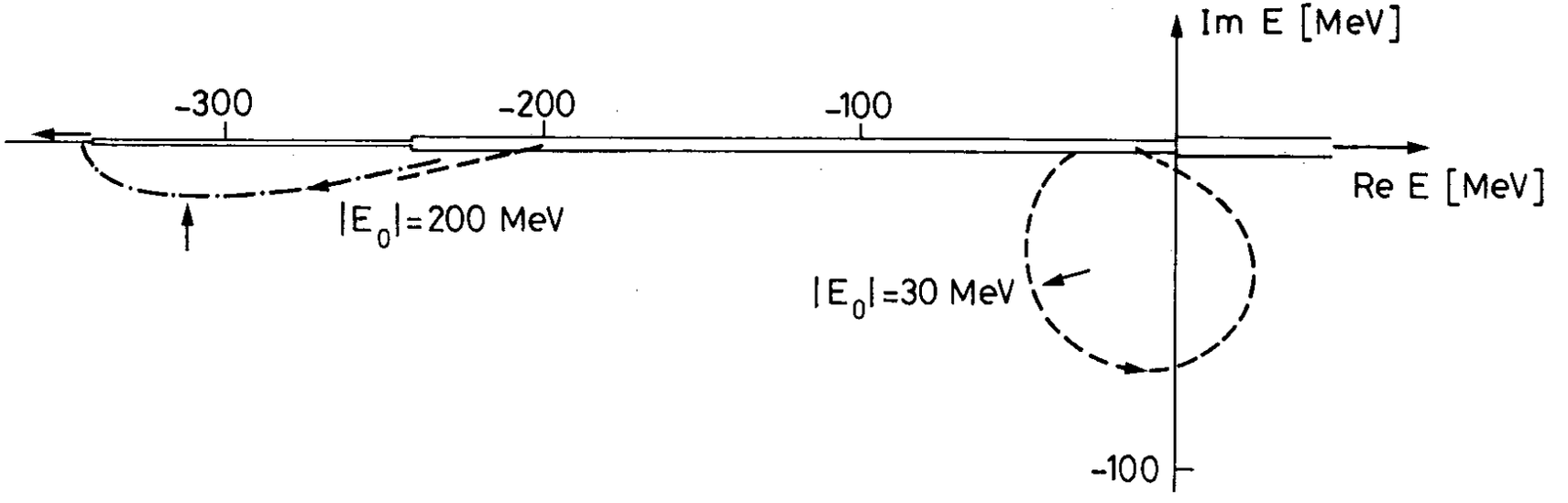
Im E [MeV]
-300
-200
-100
Re E [MeV]
$|E_0|$=200 MeV
$|E_0|$=30 MeV
-100

(a)

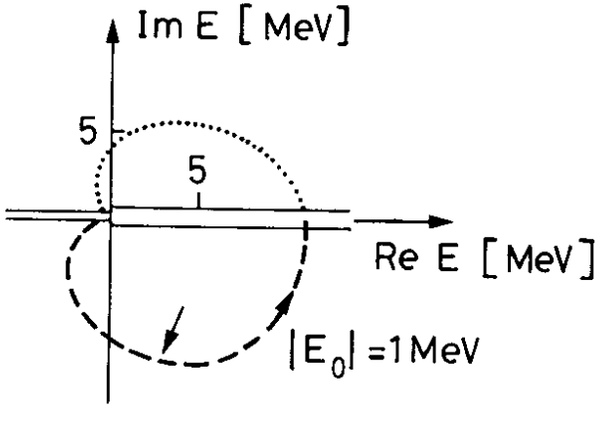
Im E [MeV]
5
5
Re E [MeV]
$|E_0|$=1 MeV

(b)

Fig. 6